Kinematic Analysis and Simulation of a Hybrid Biped Climbing Robot

Adrián Peidró, Arturo Gil, José María Marín, Yerai Berenguer and Óscar Reinoso
Systems Engineering and Automation Department, Miguel Hernández University, 03202, Elche, Spain

Keywords: Biped Robots, Climbing Robots, Hybrid Serial-parallel Robots, Kinematics, Redundant Robots, Simulation.

Abstract: This paper presents a novel climbing robot that explores 3-D truss structures for maintenance and inspection tasks. The robot is biped and has a hybrid serial-parallel architecture since each leg is composed of two parallel mechanisms connected in series. First, the forward kinematic problem of the complete robot is solved, obtaining the relative position and orientation between the feet in terms of the ten joint coordinates of the robot. The inverse kinematics is more complex due to the redundancy of the robot. Hence, a simplified inverse kinematic problem that assumes planar and symmetric movements is analyzed. Then, a tool to simulate the kinematics of the robot is presented, and it is used to demonstrate that the robot can completely explore 3-D structures, even when some movements are restricted to be planar and symmetric.

1 INTRODUCTION

Vertical structures such as buildings, bridges, silos, or towers require periodic maintenance and inspection operations. For example, the glass facades of skyscrapers must be cleaned, and the welded unions in the metallic skeletons of the buildings must be examined. Tasks like these are very dangerous for human operators, who must work in environments often difficult to access and are exposed to many risks such as falling from height, contamination (e.g. inspections in nuclear or chemical facilities) or electrocution (e.g. maintenance of power transmission lines). To eliminate these risks, during the last two decades many researchers have been investigating the possibility of automating the execution of these tasks using climbing robots. (Schmidt and Berns, 2013) present an exhaustive analysis of the applications and design criteria of climbing robots, as well as a comprehensive review of the main locomotion and adhesion technologies.

Three-dimensional truss structures are present in many vertical structures such as bridges, towers and skeletons of buildings. These structures are typically constituted by a network of beams connected at structural nodes, and a high degree of mobility is often required to explore them. Climbing robots for 3-D trusses can be classified into two main types (Tavakoli et al., 2011): continuous-motion and step-by-step robots. Continuous-motion robots are faster, use wheels, and employ magnetism or friction to adhere to the structure (Baghani et al., 2005; Tavakoli et al., 2013). However, they usually have more difficulties to negotiate obstacles and their wheels may slip. Step-by-step robots have two grippers connected by a kinematic chain which has some degrees of freedom (DOF). Their name reflects their locomotion method: in each motion cycle, one gripper is fixed to the structure, whereas the kinematic chain moves the other gripper to the next attachment point of the structure, where it will be fixed. Then, the previously fixed gripper is released and a new motion cycle begins. During each motion cycle, these robots are equivalent to typical robot manipulators. Hence, they have a higher mobility that facilitates the avoidance of obstacles, but they are heavier, slower, and more complex.

The architecture of the kinematic chain of step-by-step robots can be serial, parallel, or hybrid. Serial architectures have larger workspaces than parallel ones, but they are less rigid and have a limited load capacity. The serial architectures have been the most explored ones in step-by-step climbing robots, with many different designs proposed by different authors. For example, (Balaguer et al., 2000) present a 6-DOF robot to explore 3-D metallic structures. Since the robot is powered by a battery, the movements are optimized to reduce the energy consumption and increase its autonomy. Another 4-DOF serial climbing robot is presented in (Tavakoli et al., 2011). Other authors propose serial architectures inspired by inchworms, with 5 and 8 DOF (Guan et al., 2011; Shvalb et al., 2013). (Mampel et al., 2009) propose a similar mod-

Peidro A., Gil A., Marin J., Berenguer Y. and Reinoso O..
Kinematic Analysis and Simulation of a Hybrid Biped Climbing Robot.
DOI: 10.5220/0005515800240034
In *Proceedings of the 12th International Conference on Informatics in Control, Automation and Robotics* (ICINCO-2015), pages 24-34
ISBN: 978-989-758-123-6

ular robot whose number of DOF can be increased connecting more modules in series. Finally, (Yoon and Rus, 2007) present 3-DOF robots that can individually explore 3-D trusses or can be combined with other robots to form more complex kinematic chains with higher maneuverability.

Parallel climbing robots are less common, but they have also been studied. These architectures offer a higher payload-to-weight ratio than serial robots, but their workspace is more limited. (Aracil et al., 2006) propose using a Gough-Stewart platform as the main body of a robot for climbing truss structures, pipelines and palm trees. The robot remains fixed to the structure using grippers or embracing it with its annular platforms.

Finally, hybrid climbing robots are composed of some serially connected parallel mechanisms, and they have the advantages of both architectures: high maneuverability, rigidity and load capacity. A hybrid robot for climbing 3-D structures is proposed by (Tavakoli et al., 2005), who combine a 3-RPR parallel robot with a rotation module connected in series. Another hybrid robot is proposed in (Figliolini et al., 2010). In this case, the robot is biped and each leg is the serial combination of two 3-RPS parallel robots. Hence, the complete robot has 12 DOF.

In this paper, we present a novel 10-DOF redundant hybrid robot for climbing 3-D truss structures. The robot is biped and its legs are connected to a hip through revolute joints. Each leg is the serial combination of two parallel mechanisms that possess linear hydraulic actuators, which provide a high load capacity and stiffness. The design of the robot makes it specially suitable to maneuver in 3-D truss structures and perform transitions between planes with different orientations. In this paper, we focus on the forward and inverse kinematic problems of the robot, which are necessary to plan trajectories in 3-D structures. We also present a Java simulation tool that allows us to verify the kinematic models obtained in this paper and demonstrate the ability of the robot to explore 3-D trusses.

This paper is organized as follows. The architecture of the robot is described in detail in Section 2. Next, the forward kinematic problem of the complete robot when one foot remains fixed is solved in Section 3. In Section 4, a simplified yet useful version of the inverse kinematic problem is solved. Then, Section 5 presents a tool that simulates the forward kinematics of the robot. This tool is used to demonstrate the execution of some example trajectories by the robot in a 3-D structure. Finally, the conclusions and future work are exposed in Section 6.

2 DESCRIPTION OF THE ROBOT

Figure 1a shows a 3-D model of the biped climbing robot. The robot has two identical legs (A and B) connected to the hip through revolute joints driven by motors (angles θ_A and θ_B). Each leg has three links: a core link and two platforms. The lower platform is the foot of the leg and carries the gripper that fixes the robot to the structure (the grippers are not considered in the kinematic analysis presented in this paper). The upper platform is connected to the hip through the aforementioned revolute joint. Each platform is connected to the core link by means of two prismatic actuators and a passive slider.

The mechanism composed of the core link, one platform, and the two prismatic actuators that connect these two elements, is a closed-loop linkage that will be called hereafter "parallel module". The parallel modules are planar mechanisms that can be represented schematically as shown in Figure 1b. Hence, each leg is the serial combination of the parallel modules 1 (which is connected to the foot) and 2 (which is connected to the hip). The prismatic actuators of each parallel module lie in opposite sides of the plane Π_j, which is one of the planes of symmetry of the core link of the leg j (see the side view in Figure 1a). This is indicated with dashed lines in Figure 2.

Figure 1a also shows some reference frames attached to different parts of the robot. In this paper, the X, Y, and Z axes of reference frames will be represented in red, green, and blue colors, respectively. The frames H_A and H_B are fixed to the hip of the robot, whereas the frames A and B are respectively attached to the feet of the legs A and B.

The robot has 10 DOF: the rotation angles θ_A and θ_B, and the four prismatic actuators of each leg. In the next sections, the forward and inverse kinematic problems of the robot will be analyzed. After that, we will simulate the forward kinematics to demonstrate its ability to explore 3-D structures.

3 FORWARD KINEMATICS

In this section, the forward kinematic problem (FKP) of the robot is solved. The problem considered here consists in calculating the position and orientation of one foot with respect to the other foot when the joint coordinates are known: the angles θ_A and θ_B and the lengths (l_{ij}, r_{ij}) of the linear actuators of the parallel modules ($i \in \{1,2\}$, $j \in \{A,B\}$). First, the forward kinematics of the parallel modules is analyzed.

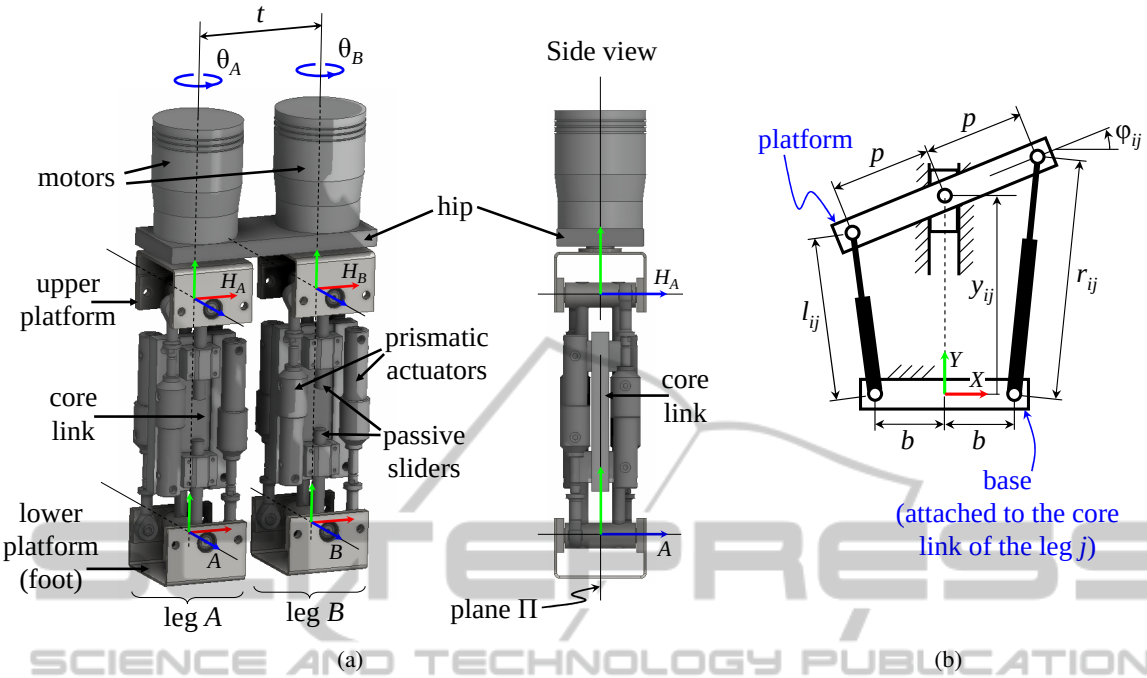

Figure 1: (a) 3-D model of the climbing robot. (b) A schematic diagram of a parallel module.

3.1 FKP of the Parallel Modules

Figure 1b shows the i-th parallel module of the leg j ($i \in \{1,2\}$, $j \in \{A,B\}$). A parallel module is a closed-loop planar mechanism composed of a mobile platform connected to a base through two prismatic actuators with lengths l_{ij} and r_{ij}. The platform is constrained to only translate vertically and rotate. The forward kinematics consists in calculating the position y_{ij} and the orientation φ_{ij} of the mobile platform in terms of l_{ij} and r_{ij}. According to Figure 1b, the relationship between (l_{ij}, r_{ij}) and (y_{ij}, φ_{ij}) is:

$$(p\cos\varphi_{ij} - b)^2 + (y_{ij} + p\sin\varphi_{ij})^2 = r_{ij}^2 \quad (1)$$

$$(p\cos\varphi_{ij} - b)^2 + (y_{ij} - p\sin\varphi_{ij})^2 = l_{ij}^2 \quad (2)$$

These equations can be combined to obtain an equivalent system. Adding together Eqs. (1) and (2) yields Eq. (3), whereas subtracting Eq. (2) from Eq. (1) results in Eq. (4):

$$4bp\cos\varphi_{ij} = 2y_{ij}^2 + 2b^2 + 2p^2 - l_{ij}^2 - r_{ij}^2 \quad (3)$$

$$4y_{ij}p\sin\varphi_{ij} = r_{ij}^2 - l_{ij}^2 \quad (4)$$

Solving $\cos\varphi_{ij}$ from Eq. (3) gives:

$$\cos\varphi_{ij} = \frac{2y_{ij}^2 + 2b^2 + 2p^2 - l_{ij}^2 - r_{ij}^2}{4bp} \quad (5)$$

Squaring Eq. (4):

$$16y_{ij}^2p^2(1 - \cos^2\varphi_{ij}) = (r_{ij}^2 - l_{ij}^2)^2 \quad (6)$$

Finally, substituting Eq. (5) into Eq. (6) yields a cubic equation in $\Upsilon_{ij} = y_{ij}^2$:

$$\Upsilon_{ij}^3 + k_2^{ij}\Upsilon_{ij}^2 + k_1^{ij}\Upsilon_{ij} + k_0^{ij} = 0 \quad (7)$$

where:

$$k_2^{ij} = 2b^2 + 2p^2 - l_{ij}^2 - r_{ij}^2 \quad (8)$$

$$k_1^{ij} = \left[(b+p)^2 - \frac{l_{ij}^2 + r_{ij}^2}{2}\right]\left[(b-p)^2 - \frac{l_{ij}^2 + r_{ij}^2}{2}\right] \quad (9)$$

$$k_0^{ij} = b^2(l_{ij} + r_{ij})^2(l_{ij} - r_{ij})^2/4 \quad (10)$$

Equation (7) always has three roots, two of which may be complex. For a given strictly positive root Υ_{ij} of Eq. (7), two solutions are obtained for $y_{ij} = \pm\sqrt{\Upsilon_{ij}}$. For each of these two values of y_{ij}, $\cos\varphi_{ij}$ is calculated from Eq. (5), whereas $\sin\varphi_{ij}$ is obtained from Eq. (4):

$$\sin\varphi_{ij} = \frac{r_{ij}^2 - l_{ij}^2}{4y_{ij}p} \quad (11)$$

Once $\cos\varphi_{ij}$ and $\sin\varphi_{ij}$ are known, φ_{ij} is unequivocally determined in $(-\pi, \pi]$. If $\Upsilon_{ij} = 0$, then $y_{ij} = 0$ and $\cos\varphi_{ij}$ is calculated using Eq. (5). However, $\sin\varphi_{ij}$ cannot be calculated from Eq. (11) since $y_{ij} = 0$. Instead, $\sin\varphi_{ij}$ is calculated as follows:

$$\sin\varphi_{ij} = \pm\sqrt{1 - \cos^2\varphi_{ij}} \quad (12)$$

obtaining two solutions. It is shown in (Kong and Gosselin, 2002), using Sturm's Theorem, that Eq. (7)

cannot have more than two non-negative roots. Since each non-negative root of Eq. (7) yields two different pairs (y_{ij}, φ_{ij}), the FKP of each parallel module has four solutions at most.

Note that swapping the values of r_{ij} and l_{ij} neither affects Eq. (7) nor Eq. (5), but it changes the sign of $\sin\varphi_{ij}$ in Eq. (11). Hence, swapping r_{ij} and l_{ij} changes the sign of φ_{ij}, leaving y_{ij} unchanged. This can be observed in Figure 1b, where swapping r_{ij} and l_{ij} is equivalent to rotating the figure π rad about the vertical Y axis. This fact will be exploited in Section 4 to analyze the inverse kinematics of the robot.

3.2 FKP of the Complete Robot

The forward kinematics of the complete robot consists in calculating the position and orientation of one foot with respect to the other foot when the ten joint coordinates are known. The problem will be solved using Homogeneous Transformation Matrices (HTMs). An HTM has the following form (Bajd et al., 2013):

$$\mathbf{T}_{m/n} = \begin{bmatrix} \mathbf{R}_{m/n} & \mathbf{t}_{m/n} \\ \mathbf{0}_{1\times 3} & 1 \end{bmatrix} \tag{13}$$

where $\mathbf{0}_{1\times 3} = [0,0,0]$. The matrix $\mathbf{T}_{m/n}$ encodes the position and orientation of a frame m with respect to another frame n. Indeed, $\mathbf{R}_{m/n} \in \mathbb{R}^{3\times 3}$ is a rotation matrix whose columns are the vectors of the frame m expressed in the basis formed by the vectors of the frame n, whereas $\mathbf{t}_{m/n} \in \mathbb{R}^{3\times 1}$ is the position of the origin of the frame m in coordinates of the frame n.

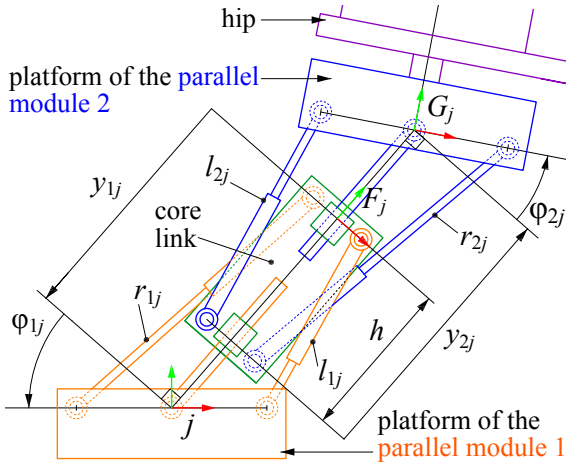

Figure 2: Kinematics of a generic leg $j \in \{A,B\}$.

The forward kinematics of one leg can be easily solved using HTMs. Figure 2 represents schematically a generic leg $j \in \{A,B\}$. Each leg has two parallel modules whose bases are attached to the core link. The platform of the parallel module 1 is the foot of the leg, whereas the platform of the parallel module 2 is connected to the hip of the robot by means of a revolute joint. The variables $(y_{1j}, \varphi_{1j}, y_{2j}, \varphi_{2j})$ are obtained from $(l_{1j}, r_{1j}, l_{2j}, r_{2j})$ as explained in Section 3.1. All the reference frames of Figure 2 are contained in the plane Π_j, which is one of the planes of symmetry of the core link of the leg j (see Figure 1a). The transformation between the frame j (fixed to the foot) and the frame F_j (fixed to the core link) is:

$$\mathbf{T}_{F_j/j} = \begin{bmatrix} \cos\varphi_{1j} & \sin\varphi_{1j} & 0 & y_{1j}\sin\varphi_{1j} \\ -\sin\varphi_{1j} & \cos\varphi_{1j} & 0 & y_{1j}\cos\varphi_{1j} \\ 0 & 0 & 1 & 0 \\ 0 & 0 & 0 & 1 \end{bmatrix} \tag{14}$$

Similarly, the transformation between the frame G_j (attached to the platform of the parallel module 2) and the frame F_j is:

$$\mathbf{T}_{G_j/F_j} = \begin{bmatrix} \cos\varphi_{2j} & -\sin\varphi_{2j} & 0 & 0 \\ \sin\varphi_{2j} & \cos\varphi_{2j} & 0 & y_{2j}-h \\ 0 & 0 & 1 & 0 \\ 0 & 0 & 0 & 1 \end{bmatrix} \tag{15}$$

where h is a geometric constant. Finally, a rotation θ_j about the Y axis of the frame G_j transforms it into the frame H_j, which is attached to the hip of the robot:

$$\mathbf{T}_{H_j/G_j} = \begin{bmatrix} \cos\theta_j & 0 & \sin\theta_j & 0 \\ 0 & 1 & 0 & 0 \\ -\sin\theta_j & 0 & \cos\theta_j & 0 \\ 0 & 0 & 0 & 1 \end{bmatrix} \tag{16}$$

The position and orientation of the frame H_j with respect to the frame j is obtained as follows:

$$\mathbf{T}_{H_j/j} = \mathbf{T}_{F_j/j}\mathbf{T}_{G_j/F_j}\mathbf{T}_{H_j/G_j} \tag{17}$$

which completes the FKP of any generic leg j. Once the forward kinematics of each leg is solved, it is straightforward to calculate the position and orientation of the foot of one leg $k \in \{A,B\} \setminus \{j\}$ with respect to the foot of the other leg j:

$$\mathbf{T}_{k/j} = \mathbf{T}_{H_j/j}\mathbf{T}_{H_k/H_j}\mathbf{T}_{k/H_k} \tag{18}$$

where $\mathbf{T}_{k/H_k} = \left(\mathbf{T}_{H_k/k}\right)^{-1}$ and $\mathbf{T}_{H_k/H_j}$ is the HTM that encodes the position and orientation of the frame H_k with respect to the frame H_j:

$$\mathbf{T}_{H_k/H_j} = \begin{bmatrix} \mathbf{I} & \mathbf{t}_{H_k/H_j} \\ \mathbf{0}_{1\times 3} & 1 \end{bmatrix} \tag{19}$$

which is constant because both frames are attached to the same rigid body (the hip). $\mathbf{I}$ is the 3×3 identity matrix. Moreover, according to Figure 1a: $\mathbf{t}_{H_B/H_A} = [t,0,0]^T = -\mathbf{t}_{H_A/H_B}$, where t is the distance between the parallel axes of the revolute actuators.

Note that, in theory, there are $4^4 = 256$ different solutions to the FKP of the complete robot. This is because the kinematic chain between the feet has four parallel modules connected in series and the FKP of each module has four real solutions at most.

4 INVERSE KINEMATICS

The inverse kinematic problem (IKP) consists in calculating the values of the joint coordinates necessary to attain a desired relative position and orientation between the feet of the robot, and it is necessary for planning trajectories. In this robot, ten joint coordinates are used to place and orient one foot with respect to the other foot, which makes it redundant. Hence, the IKP is underconstrained and one should expect infinitely many solutions. This redundancy makes it difficult to solve the general IKP of this robot. Fortunately, many important movements necessary to explore a 3-D structure (e.g., walking in one dimension, changing between planes, etc) can be executed using the configuration analyzed in this section, which reduces the number of variables and simplifies remarkably the IKP.

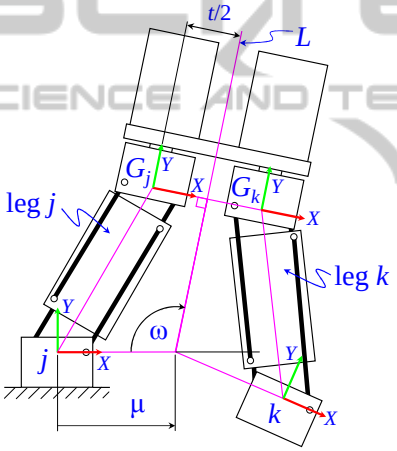

Figure 3: The Planar Symmetric Inverse Kinematic (PSIK) problem.

The configuration considered in this section is depicted in Figure 3, where the foot j is fixed to the structure and the foot k is mobile ($j,k \in \{A,B\}, j \neq k$). It is assumed that the Z axes of the frames attached to the feet are parallel and point in the same direction. Hence, any variation in the length of the prismatic actuators of the parallel modules only produces planar motions of the frame k in the XY plane of the frame j. In this case, the position and orientation of the frame k relative to the frame j can be calculated as follows:

$$\mathbf{T}_{k/j} = \mathbf{T}_{G_j/j} \begin{bmatrix} \mathbf{I} & [t,0,0]^T \\ \mathbf{0}_{1\times 3} & 1 \end{bmatrix} \left(\mathbf{T}_{G_k/k}\right)^{-1} \quad (20)$$

where $\mathbf{T}_{G_j/j} = \mathbf{T}_{F_j/j}\mathbf{T}_{G_j/F_j}$. Moreover, it is assumed that the joint coordinates of the parallel modules of the two legs are related as follows:

$$l_{ik} = r_{ij}, \quad r_{ik} = l_{ij} \quad (i = 1,2) \quad (21)$$

This means that the joint coordinates of the parallel module i of the legs k and j are swapped. According to Section 3.1, this translates into:

$$y_{ik} = y_{ij}, \quad \varphi_{ik} = -\varphi_{ij} \quad (i = 1,2) \quad (22)$$

It can be graphically checked that Eq. (22) implies that the legs k and j are symmetric with respect to the line L, which is the axis of symmetry of the hip of the robot. Substituting Eq. (22) into Eq. (20), the matrix $\mathbf{T}_{k/j}$ can be written only in terms of the variables of the leg j and has the following expression:

$$\mathbf{T}_{k/j} = \begin{bmatrix} -c(2\omega) & -s(2\omega) & 0 & \mu(1-c(2\omega)) \\ s(2\omega) & -c(2\omega) & 0 & \mu \cdot s(2\omega) \\ 0 & 0 & 1 & 0 \\ 0 & 0 & 0 & 1 \end{bmatrix} \quad (23)$$

where $s(x) = \sin x$, $c(x) = \cos x$ and:

$$\mu = \frac{t - 2(h - y_{1j} - y_{2j})\sin\varphi_{2j}}{2\cos(\varphi_{1j} - \varphi_{2j})} \quad (24)$$

$$\omega = \varphi_{1j} - \varphi_{2j} + \pi/2 \quad (25)$$

Thus, under the condition of planar and symmetric motion, the position and orientation of the foot k relative to the foot j can be defined by two parameters (μ, ω), which are indicated in Figure 3. We define the Planar Symmetric Inverse Kinematic (PSIK) problem, which consists in calculating the joint coordinates $(l_{1j}, r_{1j}, l_{2j}, r_{2j})$ needed to achieve a desired position and orientation (μ, ω). Since the joint coordinates do not appear explicitly in Eqs. (24)-(25), the kinematic equations of the parallel modules of the leg j must be included:

$$(p\cos\varphi_{1j} - b)^2 + (y_{1j} + p\sin\varphi_{1j})^2 = r_{1j}^2 \quad (26)$$

$$(p\cos\varphi_{1j} - b)^2 + (y_{1j} - p\sin\varphi_{1j})^2 = l_{1j}^2 \quad (27)$$

$$(p\cos\varphi_{2j} - b)^2 + (y_{2j} + p\sin\varphi_{2j})^2 = r_{2j}^2 \quad (28)$$

$$(p\cos\varphi_{2j} - b)^2 + (y_{2j} - p\sin\varphi_{2j})^2 = l_{2j}^2 \quad (29)$$

Hence, the PSIK problem requires calculating $(l_{1j}, r_{1j}, l_{2j}, r_{2j}, y_{1j}, \varphi_{1j}, y_{2j}, \varphi_{2j})$ from Eqs. (24)-(29). Like the general inverse kinematic problem, the PSIK problem is underconstrained since eight unknowns must be obtained from six equations. However, the PSIK problem involves less variables and simpler equations. In the following section, we will show that some postures necessary to negotiate obstacles in a 3-D structure can be analyzed solving the PSIK problem. Also, we will describe a method to choose appropriate solutions to the PSIK problem assuming that the lengths of the prismatic actuators of the parallel modules have upper and lower limits.

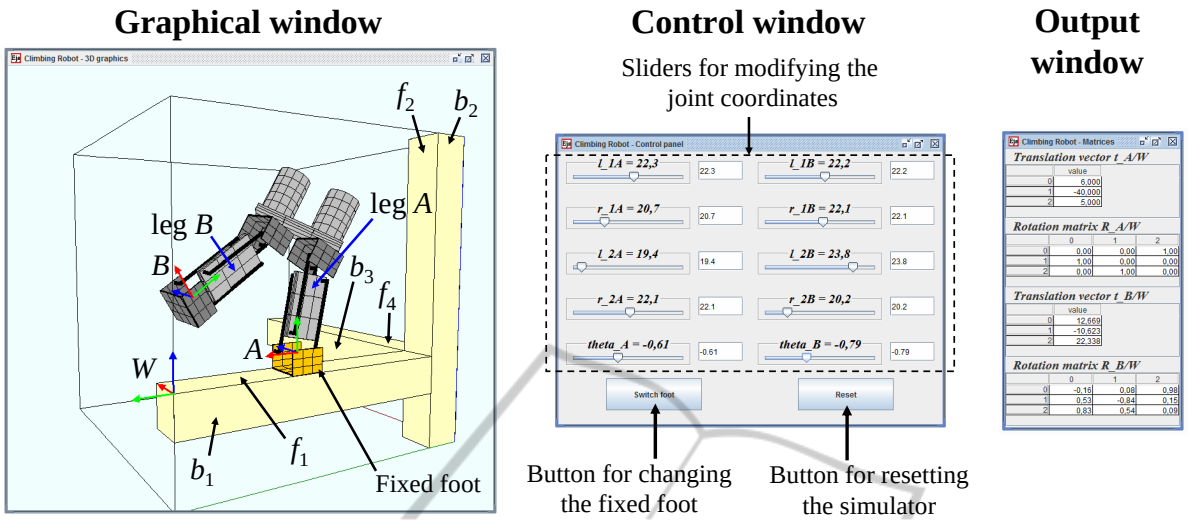

Figure 4: Interface of the tool developed to simulate the forward kinematics of the robot.

5 SIMULATION

In this section, we will simulate the movements of the complete robot in an example 3-D structure to validate the kinematic analyses of Sections 3 and 4, and demonstrate the ability of the robot to explore the structure. More specifically, we will show how the robot can walk on a beam, perform transitions between different faces of the beams, and negotiate structural nodes.

To demonstrate these movements, we have developed a Java simulation tool that can be downloaded from http://arvc.umh.es/parola/climber.html (the latest version of Java may be required). The simulator implements the equations derived in Section 3 to solve the forward kinematics. As shown in Figure 4, the simulator has a graphical window that shows the robot in the 3-D test structure. The tool also has a window with a control panel where the user can modify the values of the ten joint coordinates, change the foot that is attached to the structure, or reset the simulation. It is important to remark that the simulation tool only implements the kinematic equations, without considering the dynamics of the robot (gravity is neglected) or the collisions between the robot and the structure. These advanced topics will be analyzed in the future.

Three reference frames are shown in the graphical window of the simulator: the world frame W (which is attached to one of the corners of the beam b_1 of the structure) and the frames A and B (which are attached to the feet of the legs). The fixed foot is indicated in orange color. When the user modifies the value of a joint coordinate, the forward kinematics is solved and the position and orientation of the free foot with respect to the frame W is calculated as follows:

$$\mathbf{T}_{k/W} = \mathbf{T}_{j/W}\mathbf{T}_{k/j} \tag{30}$$

where the matrix $\mathbf{T}_{k/j}$ is defined in Section 3.2, j denotes the fixed leg, and k denotes the mobile leg ($j,k \in \{A,B\}$, $j \neq k$). As shown in Figure 4, the translation and rotation submatrices of $\mathbf{T}_{A/W}$ and $\mathbf{T}_{B/W}$ are indicated to the user in an output window of the simulator. According to Section 3.2, there are 256 solutions to the forward kinematics of the complete robot since each parallel module can have up to four different solutions. However, it will be shown next that only one solution is valid.

For the following simulations, we will assume that $b = p = 4$ cm, and that the prismatic actuators are constrained so that $r_{ij}, l_{ij} \in [19,25]$ cm. Solving the forward kinematics of a parallel module for these ranges of the joint coordinates, and plotting the solution y_{ij} versus r_{ij} and l_{ij}, results in the four surfaces shown in Figure 5. Each surface is associated with one of the configurations labeled as follows: H^+, X^+, H^-, and X^-. The solutions H^+ and X^+ are indicated in Figure 5; the solutions H^- and X^- are their respective mirror images with respect to the base of the parallel module. According to the design of the robot (see Section 2), the only valid solution is H^+, since the other solutions are impossible due to mechanical interferences between different links of the legs. Moreover, Figure 5 also provides a criterion for selecting the valid solution: the solution H^+ always has the highest y_{ij} coordinate.

Once the only valid solution to forward kinematics has been characterized, we will simulate the execution of an example trajectory in the structure, which is

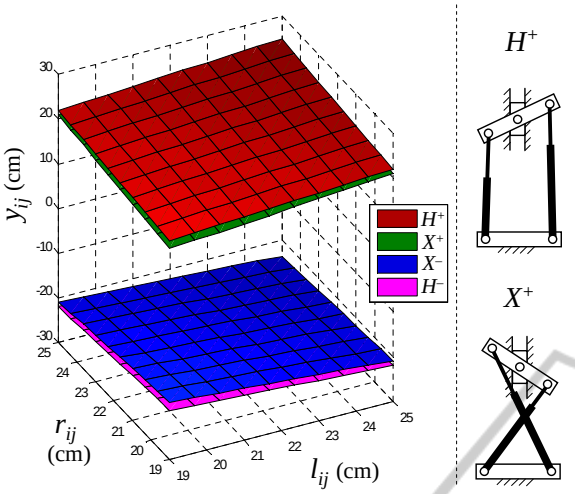

Figure 5: Solution surfaces of the FKP of a parallel module for $b = p = 4$ cm. The surfaces H^+ and H^- are almost parallel to the surfaces X^+ and X^-, respectively.

composed of the three beams b_1, b_2, and b_3 indicated in Figure 4. At the beginning of the trajectory, the robot lies on the face f_1 of the beam b_1, and the objective is to move the robot to the face f_4 of the beam b_3, negotiating the structural node where the three beams intersect. Next, we will show that such a trajectory can be executed by a sequence of basic movements that can be used to reach any other point of the structure. The values of the remaining geometric parameters of the robot are: $t = 15.6$ cm, $h = 16$ cm. Moreover, the side of the square cross section of the beams measures 12 cm, and the distance between the face f_2 of the beam b_2 and the origin of the frame W is 88 cm.

5.1 Phase 1: Walking Along a Beam

At the beginning of the trajectory (see Figure 6a), the foot A is attached to the face f_1 of the beam b_1, and the frame A has the following position and orientation:

$$\mathbf{t}_{A/W} = \begin{bmatrix} 6 \\ -40 \\ 5 \end{bmatrix} \text{cm}, \; \mathbf{R}_{A/W} = \begin{bmatrix} 0 & 0 & 1 \\ 1 & 0 & 0 \\ 0 & 1 & 0 \end{bmatrix} \quad (31)$$

The number "6" in $\mathbf{t}_{A/W}$ means that the frame A is centered in the beam, whereas the number "5" is a geometric constant of the feet of the robot. Initially, the joint coordinates have the following values: $\theta_A = \theta_B = 0$, $r_{ij} = l_{ij} = 21$ cm ($i \in \{1,2\}$, $j \in \{A,B\}$). Starting from this configuration, Table 1 describes a simple sequence of movements that allows the robot to reach the vertical beam b_2. In each step of the given sequence, we indicate only the joint coordinates that change with respect to the previous step.

5.2 Phase 2: Concave Change of Plane

Once the beam b_2 has been reached, it can be climbed to negotiate the structural node defined by the intersection of the three beams. The next objective is to perform a concave transition between the faces f_1 and f_2. Note that at the end of the previous phase (Figure 6f), the Z axes of the frames attached to the two feet point in the same direction. Hence, the postures needed to change between these faces can be obtained solving the PSIK problem defined in Section 4.

Figure 7a indicates the input parameters needed to solve the PSIK problem: $\mu = 27.4$ cm, $\omega = \pi/4$ rad, and $j = B$. Substituting these values and the geometric parameters of the robot into Eqs. (24)-(29) yields:

$$\frac{15.6 - 2(16 - y_{1B} - y_{2B})\sin\varphi_{2B}}{2\cos(\varphi_{1B} - \varphi_{2B})} = 27.4 \quad (32)$$

$$\varphi_{2B} - \pi/4 = \varphi_{1B} \quad (33)$$

$$(4\cos\varphi_{1B} - 4)^2 + (y_{1B} + 4\sin\varphi_{1B})^2 = r_{1B}^2 \quad (34)$$

$$(4\cos\varphi_{1B} - 4)^2 + (y_{1B} - 4\sin\varphi_{1B})^2 = l_{1B}^2 \quad (35)$$

$$(4\cos\varphi_{2B} - 4)^2 + (y_{2B} + 4\sin\varphi_{2B})^2 = r_{2B}^2 \quad (36)$$

$$(4\cos\varphi_{2B} - 4)^2 + (y_{2B} - 4\sin\varphi_{2B})^2 = l_{2B}^2 \quad (37)$$

As discussed in Section 4, infinitely many solutions exist since there are eight variables to be solved from six equations. Next, we describe a way of choosing a proper solution to this underconstrained problem. First, Eq. (33) is used to eliminate φ_{1B} from Eq. (32). Then, φ_{2B} is solved from the resulting equation:

$$\varphi_{2B} = \sin^{-1}\left(\frac{13.7\sqrt{2} - 7.8}{y_{1B} + y_{2B} - 16}\right) \quad (38)$$

This solution can be substituted into Eqs. (33)-(37) to express the joint coordinates $\{l_{1B}, r_{1B}, l_{2B}, r_{2B}\}$ in terms of $\{y_{1B}, y_{2B}\}$, which can be chosen so that $l_{iB}, r_{iB} \in [19, 25]$ ($i = 1, 2$). Figure 8 represents the curves of the (y_{1B}, y_{2B}) plane in which each joint coordinate equals 19 or 25; any point inside the shaded region R enclosed by these curves is a valid solution to the PSIK problem. For example, the solution $y_{1B} = y_{2B} = 22$ cm yields: $r_{1B} \approx 20.59536194$, $l_{1B} \approx 23.40761347$, $r_{2B} \approx 23.65623783$, and $l_{2B} \approx 20.34961301$, all in cm (these accurate values are valid only for the simulation; in a real implementation we will have to deal with the finite precision of the sensors). This solution is used to perform a transition between the faces f_1 and f_2 (see Figure 7a). After performing this transition, the foot A is attached to the beam b_2, and the sequence of movements described in Table 2 is used to complete this phase.

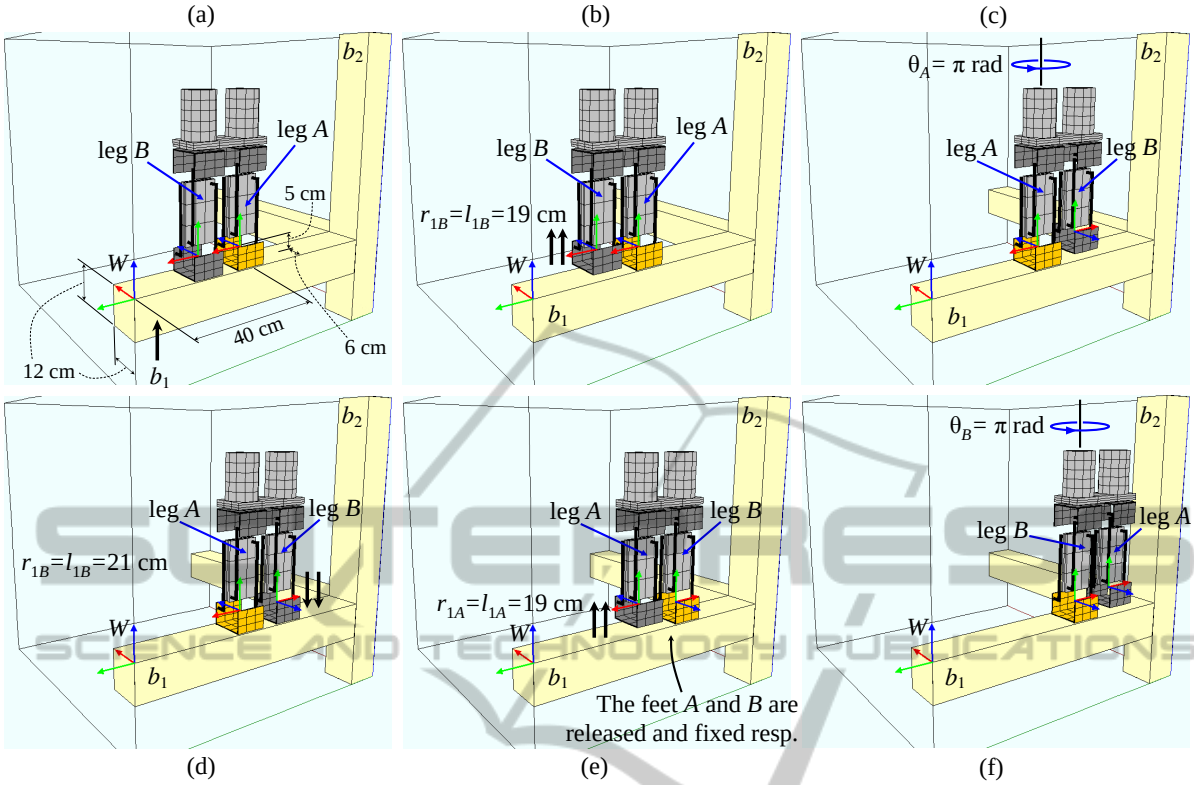

Figure 6: Example trajectory where the robot moves along a beam of the structure.

Table 1: Sequence of movements in the first phase of the simulated trajectory.

Step	Joint coordinates	Description of the movements in each step
1	$r_{1B} = l_{1B} = 19$ cm	Retract the actuators connected to the foot B to lift it (Figure 6b).
2	$\theta_A = \pi$ rad	Rotate the robot about the leg A (Figure 6c).
3	$r_{1B} = l_{1B} = 21$ cm	Extend the actuators connected to the foot B until it touches the beam b_1 (Figure 6d).
4	$r_{1A} = l_{1A} = 19$ cm	Attach the foot B to the face f_1. Release and lift the foot A retracting the actuators connected to it (Figure 6e).
5	$\theta_B = \pi$ rad	Rotate the robot about the leg B (Figure 6f).

Table 2: Sequence of movements in the second phase of the simulated trajectory.

Step	Joint coordinates	Description of the movements in each step
1	$l_{iA} = r_{iA} = 21$ cm $l_{2B} = r_{2B} = 21$ cm $l_{1B} = r_{1B} = 19$ cm	Lift the foot B and place both legs perpendicular to the face f_2, leaving some distance between the foot B and the face f_2 (Figure 7b).
2	$\theta_B = \pi/2$ rad	Rotate the leg B about its own axis (Figure 7c).
3	$r_{1B} = l_{1B} = 21$ cm	Extend the actuators connected to the foot B until it touches the face f_2 (Figure 7d).
4	$r_{1A} = l_{1A} = 19$ cm	Attach the foot B to the face f_2. Release and lift the foot A retracting the actuators connected to it (Figure 7e).
5	$\theta_B = \pi$ rad	Rotate the robot about the leg B (Figure 7f).

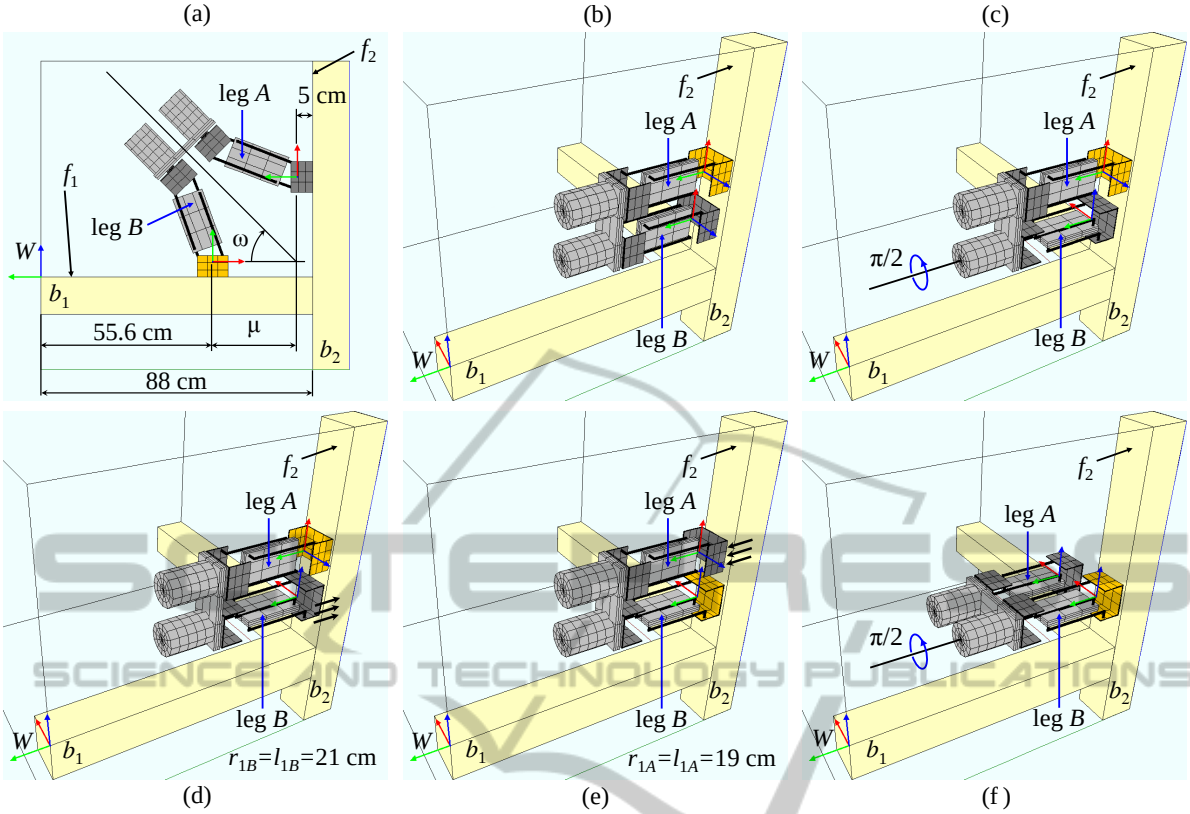

Figure 7: A trajectory that includes a concave transition between different planes.

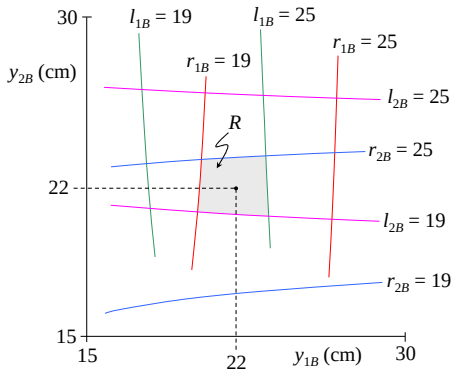

Figure 8: Region of valid solutions to the PSIK problem.

5.3 Phase 3: Convex Change of Plane

At the end of phase 2, the Z axes of the frames attached to the feet are parallel to the beam b_2 and point in the same direction. Hence, the PSIK problem can be solved to determine the joint coordinates that permit performing a convex transition from the face f_2 to the face f_3 (the face f_3 is defined in Figure 9). Substituting $\mu = 11$ cm, $\omega = 3\pi/4$ rad, and $j = B$ in Eqs. (24)-(29), and following the procedure detailed in Section 5.2, we can obtain the region of the (y_{1B}, y_{2B}) plane where $l_{iB}, r_{iB} \in [19, 25]$ cm ($i = 1, 2$). It can be checked that the solution adopted in the previous section ($y_{1B} = y_{2B} = 22$ cm) is also valid here, obtaining in this case: $r_{1B} \approx 24.85374622$, $l_{1B} \approx 19.20940403$, $r_{2B} \approx 21.99688208$, and $l_{2B} \approx 22.00311791$ (all in cm). For these values of the joint coordinates, the robot can perform a transition between the faces f_2 and f_3 (see Figure 9a). After that, the foot A can be attached to the face f_3.

After attaching the foot A to the face f_3, the sequence of movements described in Table 3 is executed. After executing this sequence, solving exactly the same PSIK problem as in Section 5.2 permits the foot A of the robot to be attached to the face f_4 of the beam b_3, which completes the trajectory.

6 CONCLUSIONS

This paper has presented the kinematic analysis of a novel biped climbing robot with a hybrid serial-parallel architecture. The forward kinematic problem was solved, obtaining the relative position and orientation between the feet in terms of the joint coordi-

Table 3: Sequence of movements in the third phase of the simulated trajectory.

Step	Joint coordinates	Description of the movements in each step
1	$l_{iA} = r_{iA} = 21$ cm $l_{2B} = r_{2B} = 21$ cm $l_{1B} = r_{1B} = 19$ cm	Place both legs perpendicular to the face f_3, leaving some distance between the foot B and the face f_3 (Figure 9b).
2	$\theta_A = 3\pi/2$ rad	Rotate the robot about the leg A (Figure 9c).
3	$r_{1B} = l_{1B} = 21$ cm	Extend the actuators connected to the foot B until it touches the face f_3 (Figure 9d).
4	$r_{1A} = l_{1A} = 19$ cm	Attach the foot B to the face f_3. Release and lift the foot A retracting the actuators connected to it (Figure 9e).
5	$\theta_A = \pi$ rad	Rotate the leg A about its own axis (Figure 9f).

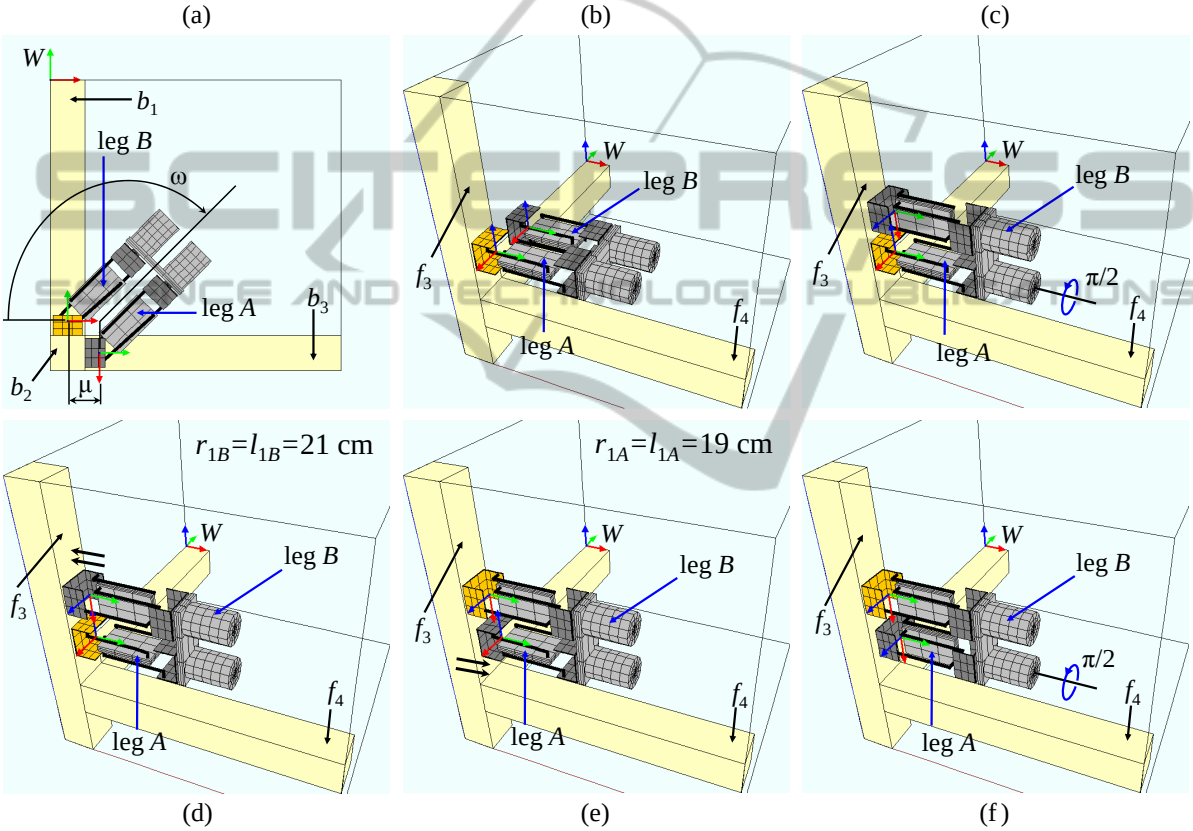

Figure 9: A trajectory that includes a convex transition between different planes.

nates. The inverse problem is more difficult due to the redundancy of the robot. Hence, a simplified inverse problem was analyzed. It was shown that the simplified problem is sufficient to perform some important trajectories which are necessary to explore 3-D structures. This was shown using a tool that simulates the kinematics of the robot and demonstrates its ability to explore 3-D trusses.

To exploit all the possibilities offered by the proposed kinematic architecture, the general inverse kinematic problem of the robot will be solved in the future. Other problems that will need to be addressed include the determination of the workspace (positions and orientations that are attainable from a given attachment point), the dynamic modeling of the robot, and the planning of trajectories avoiding collisions. Also, the performance of the robot will be studied in more complex structures (with beams having arbitrary orientation, not just orthogonal frames), and a real prototype of the robot is currently being developed to test it in a real structure.

ACKNOWLEDGEMENTS

This work was supported by the Spanish Government through the Ministerio de Educación, Cultura y Deporte under a FPU grant (Ref: FPU13/00413) and through the Ministerio de Economía y Competitividad under Project DPI2013-41557-P.

REFERENCES

Aracil, R., Saltaren, R. J., and Reinoso, O. (2006). A climbing parallel robot: a robot to climb along tubular and metallic structures. *IEEE Robotics & Automation Magazine*, 13(1):16–22.

Baghani, A., Ahmadabadi, M. N., and Harati, A. (2005). Kinematics Modeling of a Wheel-Based Pole Climbing Robot (UT-PCR). In *Proceedings of the 2005 IEEE International Conference on Robotics and Automation*, pages 2099–2104.

Bajd, T., Mihelj, M., and Munih, M. (2013). *Introduction to Robotics*. Springer Netherlands.

Balaguer, C., Giménez, A., Pastor, J. M., Padrón, V. M., and Abderrahim, M. (2000). A climbing autonomous robot for inspection applications in 3D complex environments. *Robotica*, 18(3):287–297.

Figliolini, G., Rea, P., and Conte, M. (2010). Mechanical Design of a Novel Biped Climbing and Walking Robot. In Parenti Castelli, V. and Schiehlen, W., editors, *ROMANSY 18 Robot Design, Dynamics and Control*, volume 524 of *CISM International Centre for Mechanical Sciences*, pages 199–206. Springer Vienna.

Guan, Y., Jiang, L., Zhu, H., Zhou, X., Cai, C., Wu, W., Li, Z., Zhang, H., and Zhang, X. (2011). Climbot: A modular bio-inspired biped climbing robot. In *Proceedings of the 2011 IEEE/RSJ International Conference on Intelligent Robots and Systems*, pages 1473–1478.

Kong, X. and Gosselin, C. M. (2002). Generation and Forward Displacement Analysis of RPR-PR-RPR Analytic Planar Parallel Manipulators. *ASME J. Mech. Design*, 124(2):294–300.

Mampel, J., Gerlach, K., Schilling, C., and Witte, H. (2009). A modular robot climbing on pipe-like structures. In *Proceedings of the 4th International Conference on Autonomous Robots and Agents*, pages 87–91.

Schmidt, D. and Berns, K. (2013). Climbing robots for maintenance and inspections of vertical structures - A survey of design aspects and technologies. *Robotics and Autonomous Systems*, 61(12):1288–1305.

Shvalb, N., Moshe, B. B., and Medina, O. (2013). A real-time motion planning algorithm for a hyper-redundant set of mechanisms. *Robotica*, 31(8):1327–1335.

Tavakoli, M., Marques, L., and De Almeida, A. T. (2011). 3DCLIMBER: Climbing and manipulation over 3D structures. *Mechatronics*, 21(1):48–62.

Tavakoli, M., Viegas, C., Marques, L., Norberto Pires, J., and De Almeida, A. T. (2013). OmniClimber-II: An omnidirectional climbing robot with high maneuverability and flexibility to adapt to non-flat surfaces. In *Proceedings of the 2013 IEEE International Conference on Robotics and Automation*, pages 1349–1354.

Tavakoli, M., Zakerzadeh, M. R., Vossoughi, G. R., and Bagheri, S. (2005). A hybrid pole climbing and manipulating robot with minimum DOFs for construction and service applications. *Industrial Robot: An International Journal*, 32(2):171–178.

Yoon, Y. and Rus, D. (2007). Shady3D: A Robot that Climbs 3D Trusses. In *Proceedings of the 2007 IEEE International Conference on Robotics and Automation*, pages 4071–4076.